Confinement Effects in Block Copolymer Modified Bicontinuous Microemulsions

ARTICLE *in* THE JOURNAL OF PHYSICAL CHEMISTRY B · APRIL 2013

Impact Factor: 3.3 · DOI: 10.1021/jp402825d · Source: PubMed

7 AUTHORS, INCLUDING:

Thorsten Auth
Forschungszentrum Jülich
29 PUBLICATIONS **469** CITATIONS
SEE PROFILE

H. Frielinghaus
Forschungszentrum Jülich
137 PUBLICATIONS **1,420** CITATIONS
SEE PROFILE

Gerhard Gompper
Forschungszentrum Jülich
299 PUBLICATIONS **7,710** CITATIONS
SEE PROFILE

THE JOURNAL OF PHYSICAL CHEMISTRY B

Article

pubs.acs.org/JPCB

Confinement Effects in Block Copolymer Modified Bicontinuous Microemulsions

Simona Maccarrone,*[,†] Dmytro V. Byelov,[‡] Thorsten Auth,[§,∥] Jürgen Allgaier,[†,§] Henrich Frielinghaus,[†] Gerhard Gompper,[§,∥] and Dieter Richter[†,§]

[†]Jülich Centre for Neutron Science (JCNS), Forschungszentrum Jülich GmbH, Outstation at FRM II, Lichtenbergstr. 1, 85747 Garching, Germany

[‡]Amsterdam Scientific Instruments, Science Park 105, 1098 XG Amsterdam, The Netherlands

[§]Institute of Complex Systems, Forschungszentrum Jülich GmbH, 52425 Jülich, Germany

[∥]Institute of Advanced Simulation, Forschungszentrum Jülich GmbH, 52425 Jülich, Germany

Supporting Information

ABSTRACT: It has been established that the addition of amphiphilic diblock copolymers has a boosting effect in bicontinuous microemulsions by decreasing the minimum amount of surfactant needed to solubilize equal volumes of oil and water. The strength of the polymer effect was found to be about twice larger than the theoretical prediction. This discrepancy is explained by confinement. Previous experimental studies always considered large oil and water domains of size d compared to the typical polymer end-to-end radius, R_{ee}. The ratio of these two parameters R_{ee}/d defines the confinement parameter. We investigated the sensitivity of the polymer influence extending the range of confinement. We combined macroscopic observations of the phase behavior with microscopic measurements of the structure by small-angle neutron scattering (SANS). Both results were compared with computer simulations on the basis of the theoretical concept of Helfrich. The simulations predict an enhanced sensitivity of the polymer at medium confinement and a reversed behavior at larger confinement. The higher sensitivity at medium confinement is only slightly visible experimentally, whereas the reversed behavior (antiboosting) is clearly present. Finally, a comparison with homopolymer addition showed a common high confinement behavior for diblock copolymers and for homopolymers.

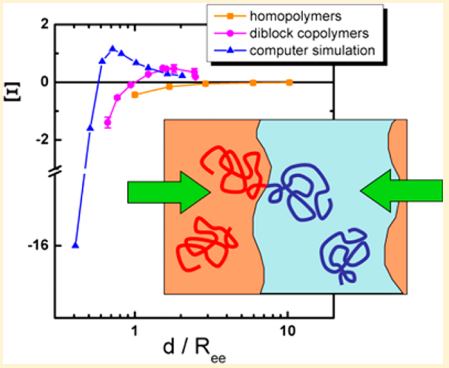

INTRODUCTION

The term microemulsion defines a thermodynamically stable mixture of oil, water, and surfactant. The two immiscible phases of oil and water are mediated by the amphiphilic molecules of the surfactant disposed in a monolayer at the interface, with the hydrophobic tails dissolved in oil and the hydrophilic head groups in water. If oil and water are present with the same amount, an alternating oil/water bicontinuous structure phase is obtained under certain conditions of temperature and surfactant concentration.[1]

The effect of polymer additives was intensively studied for their capability to modify the phase behavior and subsequently the structural properties. For instance, small amounts of amphiphilic diblock copolymer have a strong boosting effect that increases the efficiency of nonionic surfactants,[2] proportional to the minimum quantity of surfactant $\tilde{\Psi}$ needed to solubilize equal volumes of oil and water. By small-angle neutron scattering, Endo et al.[3,4] revealed that the polymer decorates the surfactant membrane and increases its stiffness. The strength of the polymer effect was found to be about 2 times larger than predicted by theory. Moreover, experiments using homopolymers[5] showed an effect seven times larger than expected.

Computer simulations were performed to quantify the effect of linear polymer chains anchored to a membrane for microemulsions in the lamellar phase. Confinement effects were taken into consideration which added the ratio of the end-to-end distance of the polymer and the microemulsion domain size R_{ee}/d to be the essential parameter as a measure for confinement. In the limit of low confinement, the simulation results confirm the classical value describing the polymer boosting effect.[6,7] But when the polymer and the microemulsions have comparable size, $R_{ee}/d \approx 0.5$, an enhanced efficiency increase is predicted, which would be interesting for applications. Intelligent additives could react on a parameter such as concentration and therefore stabilize the microemulsion under desired conditions. The presence of the polymer at the membrane is enhanced due to the confinement. At high confinement ($R_{ee}/d > 1$) a reversed behavior with decreased

Received: March 22, 2013
Revised: April 19, 2013

   dx.doi.org/10.1021/jp402825d | J. Phys. Chem. B XXXX, XXX, XXX−XXX

efficiency is found. In this limit, the anchoring of the polymer should not play a role anymore and the decreased efficiency should be a common feature whatever the kind of polymer is. The aim of the present work is to verify experimentally this picture for bicontinuous microemulsions and to explain the discrepancies encountered in previous works[3−5] in terms of confinement combining phase diagrams and small-angle neutron scattering (SANS) measurements. It is clear that the addition of the polymer influences the elastic properties of the membrane but the question we want to answer is if this influence might be diminished or amplified by the geometry of the microscopic structure.

Oil and water are considered as continuum liquids and the interfacial surfactant membrane is treated on a mesoscopic scale as a flexible sheet.[8] The curvature energy of the surfactant monolayer can be written as follows:

$$F = \int \mathrm{d}S\, [2\kappa(H - c_0)^2 + \bar{\kappa}K] \tag{1}$$

The integral is performed over the whole interface S. $H = (c_1 + c_2)/2$ is the mean curvature and $K = c_1c_2$ is the Gaussian curvature, where c_1 and c_2 are the principal curvatures (the inverse principal radii of curvature). c_0 is the spontaneous curvature, κ is called bending rigidity, and $\bar{\kappa}$ is saddle-splay or Gaussian modulus. The former describes how much energy is necessary to change the mean curvature away from the spontaneous curvature and the latter determines the energy cost to create a saddle-type deformation.

Polymers anchored to membranes modify their elasticity. In the *mushroom* regime (low polymer density on the membrane), the polymer coils do not interact and fluctuate independently. In this case, the radius of the polymer is proportional to the end-to-end distance of the coil in bulk. The effective bending rigidity and the effective saddle-splay modulus will depend linearly on the grafting density defined as

$$\sigma = \rho_\mathrm{P} a \frac{N_\mathrm{A}}{M_\mathrm{W}} \frac{\delta}{1-\delta}$$

ρ_P is the density of the polymer, a the thickness of the membrane, N_A Avogadro's number, M_W the molecular weight of the polymer chain, and δ the volume fraction of the polymer with respect to the total amphiphile. σ counts the number of polymers per membrane area.

Qualitatively, the effect of diblock copolymer anchoring can be understood in terms of the entropy. When the polymers are homogeneously tethered to the membrane, both the membrane and neighboring polymers restrict the number of configurations which are accessible to the polymer. This should cause entropic repulsion suppressing the membrane fluctuations. Furthermore, diblock copolymers make saddle shape deformations unfavorable.

The renormalized curvature-elastic moduli can be expressed as sum of three terms:

$$\frac{\kappa_\mathrm{R}}{k_\mathrm{B}T} = \frac{\kappa_0}{k_\mathrm{B}T} + \frac{\alpha}{4\pi}\ln(\Psi) + \Xi\sigma({R_\mathrm{W}}^2 + {R_\mathrm{O}}^2) \tag{2a}$$

$$\frac{\bar{\kappa}_\mathrm{L}}{k_\mathrm{B}T} = \frac{\bar{\kappa}_0}{k_\mathrm{B}T} + \frac{\bar{\alpha}}{4\pi}\ln(\Psi) - \bar{\Xi}\sigma({R_\mathrm{W}}^2 + {R_\mathrm{O}}^2) \tag{2b}$$

where κ_0 and $\bar{\kappa}_0$ are the intrinsic moduli of the bare membrane, the second terms come from considering the influence of thermal fluctuations on shorter length scales,[9] and the third terms have been calculated for a membrane with polymers in the mushroom regime without confinement.[10] The analytical results for the sensitivity coefficients of the variation of κ and $\bar{\kappa}$ respectively with the presence of the polymer are $\Xi = (1/12)[1 + (\pi/2)] \approx 0.214$ and $\bar{\Xi} = 1/6 \approx 0.167$ for ideal linear chains.[11] For self-avoiding linear chains, $\Xi = 0.200$ and $\bar{\Xi} = 0.153$ have been obtained numerically.[6] The increased repulsion between the chains in star polymers additionally amplifies the effect per chain.[7] R_W and R_O are the end-to-end distances of the respective oil and water-soluble blocks and σ is the grafting density of the polymer. The renormalization prefactors α and $\bar{\alpha}$ are known to be 3 and 10/3.[9]

THEORETICAL SECTION

Polymers next to spherically and cylindrically deformed walls have been widely used to calculate universal values for the effect of curvature on the conformational entropy of a single chain.[6,10−12] The changes of the chain's entropy can be translated to polymer effects on the membrane's curvature elastic constants. Simulations along the lines of ref 6 have been performed for a single grafted ideal chain, confined by a planar wall that is parallel to the wall to which the chain is grafted. To estimate the curvature effects, virtual spheres and cylinders have been applied to both walls. Data for the effect on the bending rigidity that has been extrapolated to vanishing bond length in order to eliminate finite size effects is provided in Table 1.

Table 1. Universal Amplitudes a_κ for the Change of the Bending Rigidity $\kappa/k_\mathrm{B}T = a_\kappa\sigma{R_\mathrm{e}}^2$ Due to the Entropy of a Single Ideal End-Grafted Polymer at Spherically and Cylindrically Deformed Walls[a]

d/R_g	$a_{\kappa,\mathrm{d}}$	$a_{\kappa,\mathrm{o}}$	$a_{\kappa,\mathrm{t}}$
1	−8 ± 2	−8 ± 2	−16 ± 4
1.25	−0.8 ± 0.3	−0.8 ± 0.3	−1.6 ± 0.6
1.5	0.27 ± 0.04	0.45 ± 0.07	0.72 ± 0.11
1.75	0.53 ± 0.03	0.62 ± 0.03	1.15 ± 0.06
2	0.49 ± 0.02	0.50 ± 0.01	0.99 ± 0.03
2.5	0.33 ± 0.01	0.34 ± 0.01	0.67 ± 0.02
3	0.271 ± 0.003	0.227 ± 0.004	0.498 ± 0.007
4	0.222 ± 0.001	0.065 ± 0.002	0.287 ± 0.003
5	0.215 ± 0.001	0.011 ± 0.001	0.226 ± 0.002

[a]The table lists the effect on the membrane that the polymer is directly anchored to (index d), the effect on the opposite membrane (index o), and the sum of both (index t). Note that the coefficients Ξ and $a_{\kappa,\mathrm{t}}$ correspond each other.

Because it is commonly accepted that polymers grafted to membranes usually increase the bending rigidity, it is interesting to note that already the single-chain entropic effect calculated with the sphere−cylinder model predicts a strong decrease of k due to polymer addition for confinements below $d \approx R_\mathrm{g}$.

In addition to the direct effect of a grafted polymer on the membranes, polymer redistribution effects due to spontaneous curvature are known to reduce the bending rigidity that is calculated using spherical and cylindrical deformations.[7,13] For a system with confinement, a further reduction of the bending rigidity may occur due to the pressure of the polymer on the membranes; see Table 2. "Bumps" of the membrane opposite to a polymer and tilting of a diblock copolymer in order to reduce the pressure and consequently local tilting of the bilayer membrane at the attachment point can also lead to an effectively lower effective bending rigidity compared to the one

dx.doi.org/10.1021/jp402825d | J. Phys. Chem. B XXXX, XXX, XXX−XXX

Table 2. Pressure of a Grafted, Linear Chain of 1000 Monomers Confined between Two Walls with Distance d

d/R_g	$p[k_BT/R_g]$
1	16.5 ± 0.5
1.25	8.4 ± 0.3
1.5	4.75 ± 0.05
1.75	2.87 ± 0.03
2	1.84 ± 0.02
2.5	0.81 ± 0.01
3	0.37 ± 0.01
4	0.070 ± 0.003
5	<0.01

obtained from the computer simulations.[14] Analogously to the sensitivity coefficient for the bending rigidity, the sentivity coefficient for the Gaussian saddle-splay modulus can be calculated; see Table 3.

Table 3. Amplitudes of the Change in the Saddle-Splay Modulus by an Ideal Polymer for the Membrane That It Is Directly Anchored to (Index d), the Opposite Membrane (Index o), and the Sum of Both (index t)[a]

d/R_g	$\bar{a}_{\kappa,d}$	$\bar{a}_{\kappa,o}$	$\bar{a}_{\kappa,t}$
1	12 ± 4	11 ± 4	23 ± 8
1.25	2.6 ± 0.8	2.2 ± 0.7	4.8 ± 1.5
1.5	0.42 ± 0.10	0.29 ± 0.11	0.71 ± 0.21
1.75	−0.15 ± 0.06	−0.22 ± 0.05	−0.37 ± 0.11
2	−0.25 ± 0.02	−0.27 ± 0.04	−0.52 ± 0.06
2.5	−0.20 ± 0.01	−0.20 ± 0.01	−0.40 ± 0.02
3	−0.199 ± 0.005	−0.18 ± 0.02	−0.38 ± 0.03
4	−0.170 ± 0.003	−0.045 ± 0.007	−0.215 ± 0.010
5	−0.165 ± 0.003	−0.007 ± 0.001	−0.158 ± 0.004

[a]Note that the coefficients $-\Xi$ and $\bar{a}_{\kappa,t}$ correspond each other.

The change of the sign of the polymer effect on the membrane curvature-elastic coefficients is not surprising, because the anchored linear (diblock co)polymers are known to increase κ and to decrease $\bar{\kappa}$, while the opposite has found for free homopolymers.[5,11] In Figure 1, the polymer density is plotted as function of the wall distance d, for high confinement the effect of the anchor on the monomer density of the grafted chain vanishes, such that no difference for the effect on the membrane is expected for high confinement. Therefore, for appropriate confinement a qualitative change of the influence of the anchored polymer on the membrane curvature elastic constants has to occur. The polymer touches the opposite wall already for larger distances that are much larger than R_g and is considerably deformed for $R_e = \sqrt{6}R_g \approx 2.45R_g$, such that the effect on the membrane curvature elastic constants is also expected to be modified for microemulsion structure sizes of about $3R_g$ to $4R_g$.

EXPERIMENTAL SECTION

A systematic study on bicontinuous microemulsions with symmetric diblock copolymer additives was carried out varying the domain size d using different chain length oils in combination with the use of two polymers in order to vary also R_{ee}. For every system, we established three values of polymer content δ defined as the mass fraction of polymer over the total amphiphile $\delta = m_P/(m_S + m_P)$, considering also the pure system without polymer ($\delta = 0$). For each δ, three

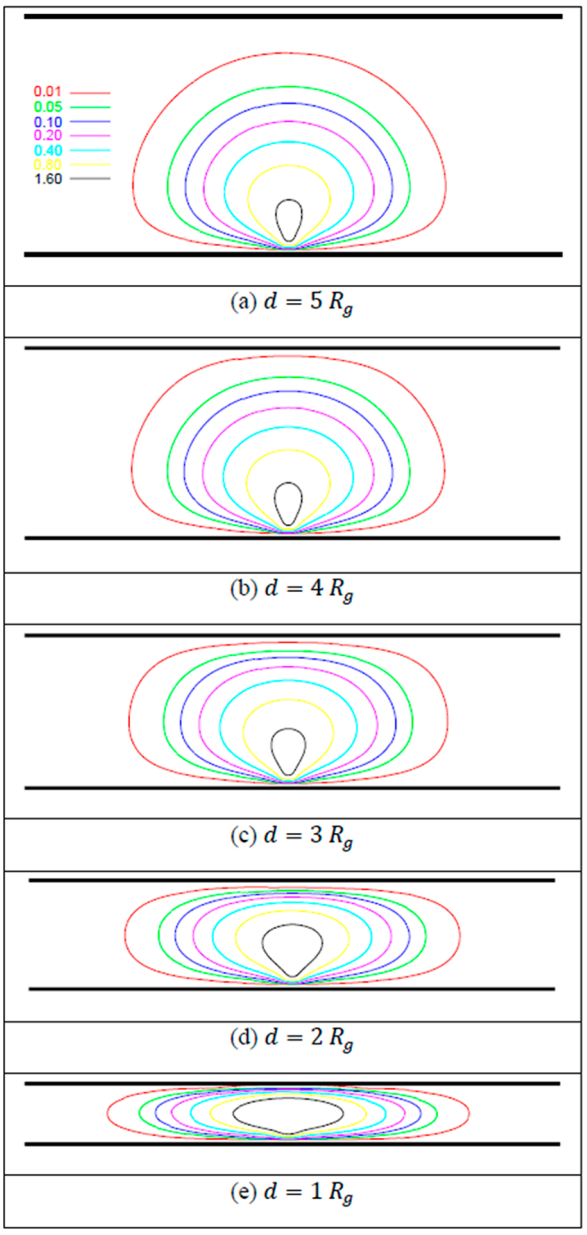

Figure 1. Contour plot of projected monomer densities of an ideal chain with 200 bonds and bond length $b = 0.1732R_g$, confined between two parallel walls at distance d. Densities are given in units of $1/b^2$.

different surfactant contents were chosen not too far from the fish-tail point $\gamma = (m_S + m_P)/(m_S + m_P + m_O + m_W)$. The microemulsions were prepared mixing equal amount of oil and water fixing the water-to-oil volume fraction $\phi_\alpha = V_O/(V_O + V_W) = 0.5$ with $V_i = m_i/\rho_i$. Particular attention is given to the membrane volume fraction Ψ defined

$$\Psi = \frac{V_S - 0.02V_O}{V_P + V_S + V_O + V_W} \quad (3)$$

where we took into account that a small percentage (2 vol %) of surfactant is solubilized in oil.[15]

As oils we chose n-alkanes C_nH_{2n+2} in the hydrogenated form (from Sigma-Aldrich and Fluka) and we substituted H_2O with D_2O (from Chemotrade) for the bulk contrast method (Table 4). We used linear-structure nonionic surfactant belonging to the poly(ethylene oxide) variety $C_{10}E_4$ purchased from Bachem

dx.doi.org/10.1021/jp402825d | J. Phys. Chem. B XXXX, XXX, XXX−XXX

Table 4. List of the Oils Used, Surfactant and Heavy Water with Their Characteristics

component	density (g/cm^3)	M_w (g/mol)
hexane C_6	0.659	86.18
heptane C_7	0.710	100.21
octane C_8	0.703	114.23
decane C_{10}	0.730	142.3
undecane C_{11}	0.740	156.31
dodecane C_{12}	0.749	170.34
tridecane C_{13}	0.756	184.37
tetradecane C_{14}	0.763	198.4
n-decyltetraoxyethylene $C_{10}E_4$	0.959	334.5
D_2O	1.105	20.02

and Fluka without further purification, in its hydrogenated form. Symmetric diblock copolymers poly(ethylenepropylene-*co*-polyethylene oxide) (PEP-PEO) of different chain length produced in our laboratory by anionic polymerization[16] were added to microemulsions (Table 5).

Table 5. List of the Polymers Used and Their Characteristics

polymer	composition	M_n[a] (g/mol)	M_w/M_n	R_W[b] (Å)	R_O[b] (Å)
$PEP_{10}PEO_{10}$	d6.25h3.75/h	21300	1.02	113	97
$PEP_{22}PEO_{22}$	d6.61h3.39/h	49000	1.03	181	159

[a]Degree of polymerization determined by size exclusion chromatography (SEC) as explained in Appendix A of ref 4. [b]End-to-end distances of the blocks obtained as in ref 4 from ref 17.

Phase Diagram Measurements. In a typical phase diagram from a nonionic surfactant that mixes equal amount of oil and water we can distinguish four regions. At low temperatures, we find an oil-in-water microemulsion coexisting with an upper oil-excess phase (labeled by $\underline{2}$), while at high temperatures a water-in-oil phase coexists with a lower water-excess phase ($\overline{2}$). At intermediate temperatures and low surfactant concentrations, a three-phase coexistence occurs composed by an upper oil-excess phase, middle phase microemulsion, and lower water-excess phase (denoted by 3) while at higher surfactant concentration water and oil are completely mixed (phase 1). The phase boundaries draw a sort of fish and the critical point in which we have the phase coexistence is the fish-tail point (FTP).

By the knowledge of the FTP coordinates $(\tilde{\Psi},\tilde{T})$, it is possible to extract information about the saddle-splay modulus $\overline{\kappa}$. It was shown[18] that the appearance of the bicontinuous phase is primarily controlled by the Gaussian modulus $\overline{\kappa}$. In particular, the phase is stable for $\overline{\kappa}_R > 0$ which becomes zero at the fish-tail point. Moreover, Monte Carlo simulations of randomly triangulated surfaces[19] demonstrated that the microemulsion coexists with excess oil and water phases under the condition:

$$\tilde{\Psi} = \exp\left[\frac{6\pi}{5}\frac{\overline{\kappa}_0}{k_BT} - \hat{\Xi}\sigma(R_W{}^2 + R_O{}^2)\right] \tag{4}$$

with $\hat{\Xi} = 4\pi\overline{\Xi}/\overline{\alpha} = \pi/5 \approx 0.628$. From eq 4 we see that the thermal fluctuations are balanced by the polymer addition and how strong the influence of the polymers is. Even if $\overline{\kappa}$ is only slightly changed, a macroscopic effect is induced due to the exponential dependence. Knowing $\tilde{\Psi}$ from the phase diagram measurements for different polymer contents and $\sigma(R_W{}^2 + R_O{}^2)$ we can easily get the coefficient $\hat{\Xi}$. Since $\hat{\Xi}$ includes the factor $4\pi/\overline{\alpha}$, our experimental coefficient should be 3.77 times larger than the net theoretical predictions of the pure polymer effect.

The phase diagram measurements were carried out in a thermal water bath.[20] One test tube containing our microemulsion is put into the bath. In there, we observe by visual inspection how the light from a lamp is scattered or polarized by the sample on varying the temperature. For this purpose, a thermostat is used, eventually connected to a bigger one that helps to reach low temperatures. At each temperature the sample is stirred and then left for a while. The one-phase regime appears completely clear while the $\underline{2}$ and $\overline{2}$ phases appear completely turbid after stirring as well as the three-phase regime but on waiting for a certain time it is possible to see the phase separation.

Small-Angle Neutron Scattering. To describe the peak of the scattering profile for bicontinuous microemulsions we used the Teubner–Strey formula[21] obtained on the basis of the Ginzburg–Landau theory

$$I(Q) = \frac{8\pi\phi_W\phi_O\Delta\rho^2/\xi}{((2\pi/d)^2 + \xi^{-2})^2 - 2((2\pi/d)^2 - \xi^{-2})Q^2 + Q^4} \tag{5}$$

where ϕ_O and ϕ_W are the volume fractions of oil and water and $\Delta\rho^2$ is the square difference of scattering length density from oil and water. d and ξ are the periodicity and the correlation length, respectively. Roughly speaking, d is related to the peak position and ξ to the peak width.

The Gaussian random field theory[22,23] as a first approach provides us a connection of these two parameters with the bending rigidity κ. In the Supporting Information, we describe the enhanced evaluation which identifies the SANS κ being a mixture of κ and $\overline{\kappa}$.[24,25] The characteristic wave vector increases linearly with the average membrane surface per unit volume $k_0 = 2\pi/d \approx S/V$, while the correlation length decreases $\xi \approx k(S/V)^{-1}$.

The dimensionless ratio of these two length scales, however, is independent of the amphiphile concentration but only depends on the bending rigidity:

$$\frac{2\pi}{d}\xi = \frac{64}{5\sqrt{3}}\frac{\kappa_R}{k_BT} \tag{6}$$

Once the domain size d and the correlation length ξ are extracted from the SANS spectra fitting, we calculate the renormalized bending rigidity from eq 6.

All the experiments were done on the small-angle neutron machine KWS2 at the FRJ-2 research reactor at the Forschungszentrum in Jülich. We used 1 mm quartz cells placed in the beam in a little furnace that kept the temperature constant for each sample. In order to cover the whole Q-range (from 0.002 to 0.2 Å^{-1}), we measured each sample at two different detector distances (between 2 and 20 m) keeping the collimation apertures distance fixed at 20 m, due to the high scattering intensity. The incident wavelength of neutrons was λ = 7.3 Å ($\Delta\lambda/\lambda$ = 0.1). The raw data were corrected for background and detector efficiency[26] and afterward calibrated in absolute units (cm^{-1}) by a Plexiglas standard.

RESULTS

Our goal was to show the role that confinement plays in bicontinuous polymer decorated microemulsions. In order to get several values of confinement, we varied d using different oils (tetradecane, tridecane, dodecane, undecane, decane,

dx.doi.org/10.1021/jp402825d | J. Phys. Chem. B XXXX, XXX, XXX–XXX

octane, and hexane)[27,28] and R_{ee} employing two diblock copolymers of different chain lengths ($PEP_{22}PEO_{22}$ and $PEP_{10}PEO_{10}$). The strategy of the experiments was to combine macroscopic observations of the phase behavior with microscopic measurements of the structure by SANS. In this way, we monitored the variation of the bending rigidity κ and the saddle-splay modulus $\bar{\kappa}$ due to the presence of the polymer.

Phase Diagram Measurements. In the one-phase region the phase boundary changes almost linearly with the surfactant amount that makes an extrapolation of the FTP easier and more exact. The $\tilde{\gamma}$ value is the x-coordinate of the intersection point of the linear fit from the upper and lower phase boundaries. Three polymer compositions δ were combined with three surfactant compositions γ around the FTP. As the same samples could be used for SANS experiments, we used directly D_2O instead of H_2O. This exchange implied a shift toward lower temperature of 2 °C.[29]

For the shorter chain oils, we found a common trend of the FTP to be shifted to lower surfactant concentrations (boosting effect). The phase inversion temperature $\tilde{T}$ stays unchanged as well as the upper and lower phase boundaries. This is due to the fact the diblock copolymers used are symmetric and they act in both oil and water phases. As an example, we consider the behavior of the hexane systems and the effect of the two different polymers (Figures 2 and 3). What we found is a

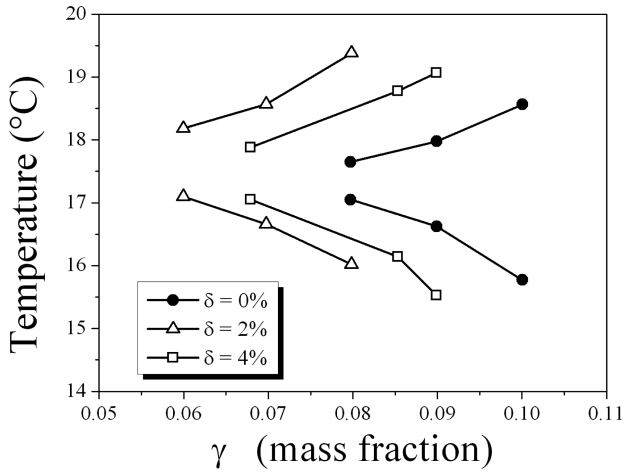

Figure 2. Phase diagram of C6–D_2O–$C_{10}E_4$–$PEP_{22}PEO_{22}$ (from SANS samples).

common enhancement for the surfactant efficiency for both cases. We extracted the amphiphile concentration $\tilde{\gamma}$ at FTP by linear fits of phase boundaries and successively we converted all mass fractions in volume fractions $\tilde{\Psi}$. In the case of the pure system, $\tilde{\Psi}$ is 0.072. This value is reduced down to 0.039 in the system with 4% of $PEP_{22}PEO_{22}$. The addition of 4% $PEP_{10}PEO_{10}$ has a similar effect with a shift to 0.041.

For the longest chain oils we did not observe the boosting effect like before. The polymer amount over the total amphiphile quantity that, staying in the one-phase region, we could add changed significantly going from the shortest chain oils (4%) up to the longest chain oils (0.025%). This small amount leaves the phase diagrams almost unchanged like in the case of dodecane systems, for example (Figure 4), for which $\tilde{\Psi}$ stays at the value of 0.146.

For the analysis, we used eq 4 written as

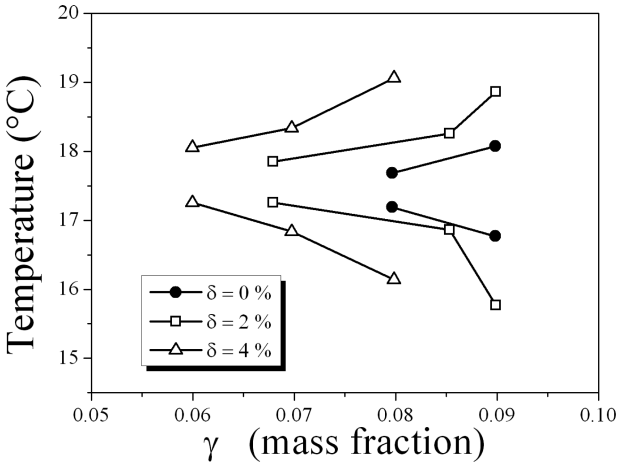

Figure 3. Phase diagram of C6–D_2O–$C_{10}E_4$–$PEP_{10}PEO_{10}$ (from SANS samples).

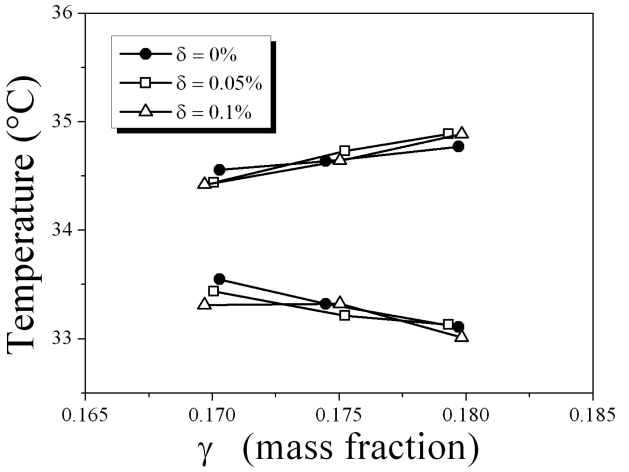

Figure 4. Phase diagram of C12–D_2O–$C_{10}E_4$–$PEP_{22}PEO_{22}$ (from SANS samples).

$$\ln\left(\frac{\tilde{\Psi}}{\tilde{\Psi}^0}\right) = -\hat{\Xi}\sigma(R_W^2 + R_O^2) \tag{7}$$

where $\tilde{\Psi}^0 = \exp(6\pi\bar{\kappa}_0/5k_BT)$ is a surfactant- and oil-dependent constant. Plotting the logarithm of the extrapolated volume fraction as a function of the polymer grafting density, it is possible to observe any variations of the sensitivity of $\bar{\kappa}$ due to the presence of the polymer at the interface.

For the short-chain oils, ln $\tilde{\Psi}$ experiences a linear decrease (slope $-\hat{\Xi}$) as it can be seen in the case of hexane systems in Figure 5. In the case of C6–D_2O–$C_{10}E_4$–$PEP_{22}PEO_{22}$, $\hat{\Xi}$ is found to be -1.65 ± 0.23 while for C6–D_2O–$C_{10}E_4$–$PEP_{10}PEO_{10}$ $\hat{\Xi}$ is -1.26 ± 0.22. For the longer chain oils, the polymer-independent surfactant volume fraction $\tilde{\Psi}$ at FTP is reflected in a slope close to zero. For instance, the C12–D_2O–$C_{10}E_4$–$PEP_{22}PEO_{22}$ systems experience a coefficient of -0.008 ± 1.98.

SANS Measurements. Our samples are characterized by two parameters: the total amphiphile mass fraction γ and the polymer mass fraction δ. It is very interesting to discuss the spectra keeping one parameter fixed while the other is varied. In this way, we directly see what happens to the domain size d and the correlation length ξ. Starting with hexane systems, we display the measured intensities for samples with and without

dx.doi.org/10.1021/jp402825d | J. Phys. Chem. B XXXX, XXX, XXX–XXX

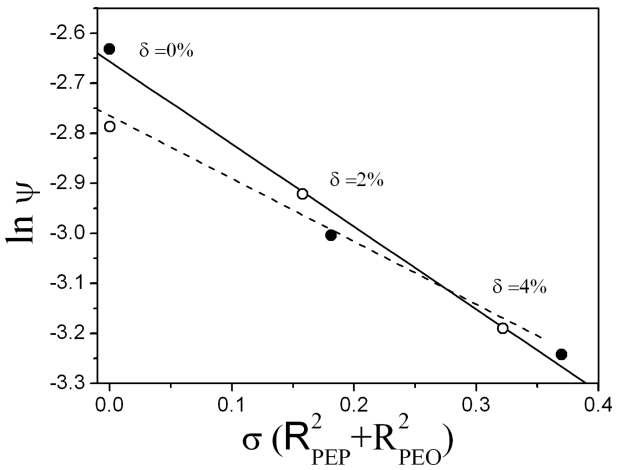

Figure 5. Membrane content vs diblock copolymer grafting density for the system C6–D_2O–$C_{10}E_4$–$PEP_{22}PEO_{22}$ (●; linear fit solid line) and C6–D_2O–$C_{10}E_4$–$PEP_{10}PEO_{10}$ (○; linear fit dash line).

polymer (Figure 6) for different amphiphile volume fractions. In both cases, a clear low-Q shift of the peak is visible as we

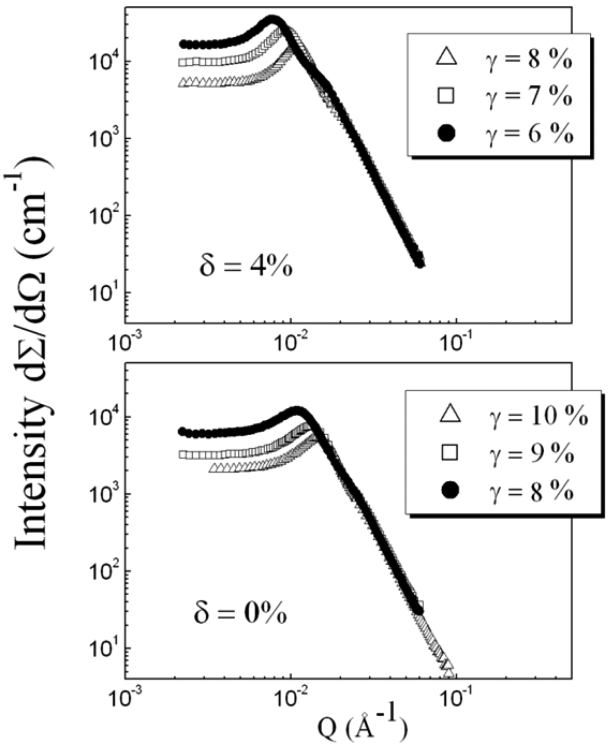

Figure 6. Comparison of the SANS spectra for C6–D_2O–$C_{10}E_4$–$PEP_{22}PEO_{22}$ systems at different polymer contents.

decrease the amphiphile fraction. From the theory we know that the peak position is related to the domain size by $k_0 = 2\pi/d$. The low-Q shift of the peak in Figure 6 means an enhancement of the domain size.

If we plot the spectra for different δ at the same value of γ, we can observe the influence on the peak width. As it can be seen in Figure 7, the presence of the polymer makes the peak sharper, which means an increase of the correlation length (inset Figure 7). Once we extracted d and ξ, we got the renormalized bending rigidity through eq 6. The presence of the polymer anchored to the interface smoothes the thermal

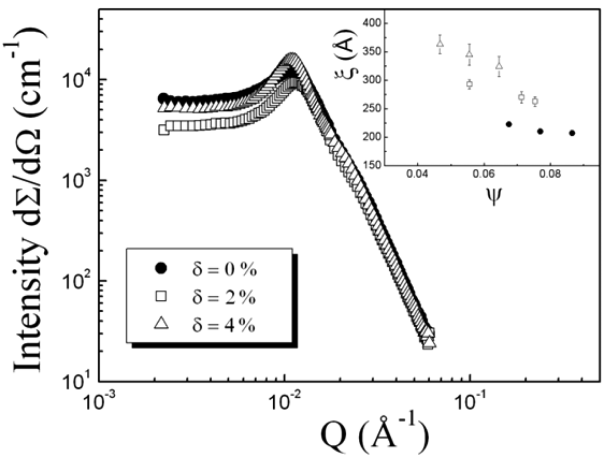

Figure 7. SANS spectra for C6–D_2O–$C_{10}E_4$–$PEP_{22}PEO_{22}$ systems with different polymer contents and $\gamma = 0.08$. A clear sharpening of the peak leads to an increasing of the correlation length as shown in the inset.

fluctuations and the membrane becomes more rigid (Figure 8). For $\Psi = 0.067$ the value of κ increases from 0.355 ($\delta = 0\%$) up

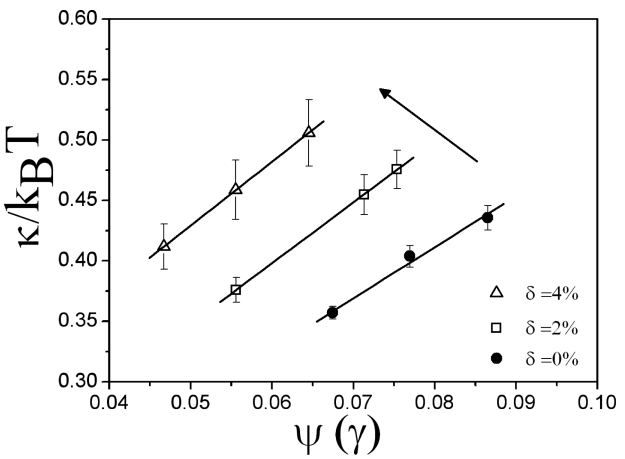

Figure 8. Renormalized bending rigidity obtained by SANS measurements for C6–D_2O–$C_{10}E_4$–$PEP_{22}PEO_{22}$ systems at different polymer contents as a function of the membrane volume fraction.

to 0.517 ($\delta = 4\%$). This tendency confirms the boosting effect observed directly from the phase diagram measurements.

For dodecane systems, we observe a completely different scenario. We saw already that there are no significant variations of the phase diagram. If we have a look at the SANS spectra, we see that the position of the peak experiences very little variation in γ (Figure 9) even in the presence of the polymer. The values of γ are quite close to each other and this implies that the domain size does not differ so much for each Ψ value.

The situation remains almost unchanged even for the width of the peak (Figure 10) where it is evident how the small quantity of polymer does not bring accordingly any variation of the correlation length ξ (inset Figure 10).

Performing the calculations for the bending rigidity, we were still able to detect a negative variation of κ on a small scale (Figure 11). For $\Psi = 0.163$ the value of κ decreases from 0.432 ($\delta = 0\%$) up to 0.420 ($\delta = 0.1\%$). The quantity of polymer is in fact quite low and the effect on the fluctuations of the membrane is very small.

dx.doi.org/10.1021/jp402825d | J. Phys. Chem. B XXXX, XXX, XXX–XXX

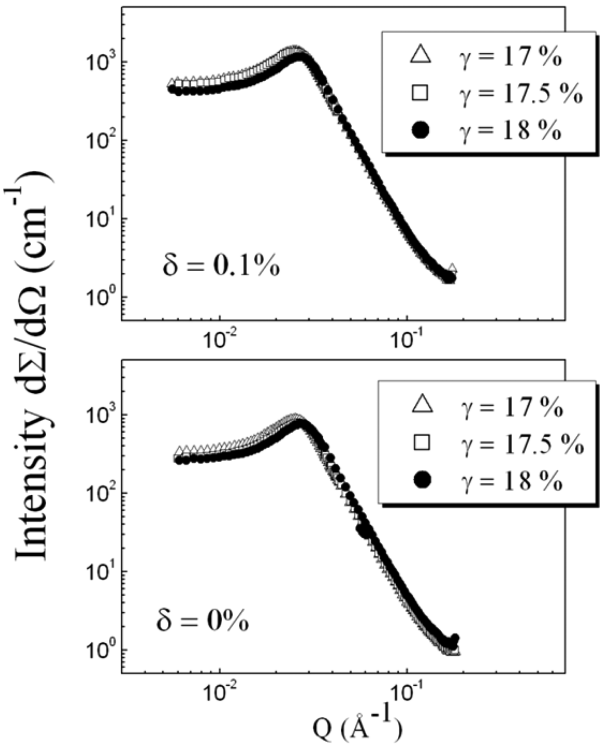

Figure 9. Comparison of the SANS spectra for C12−D_2O−$C_{10}E_4$−$PEP_{22}PEO_{22}$ systems at different polymer contents.

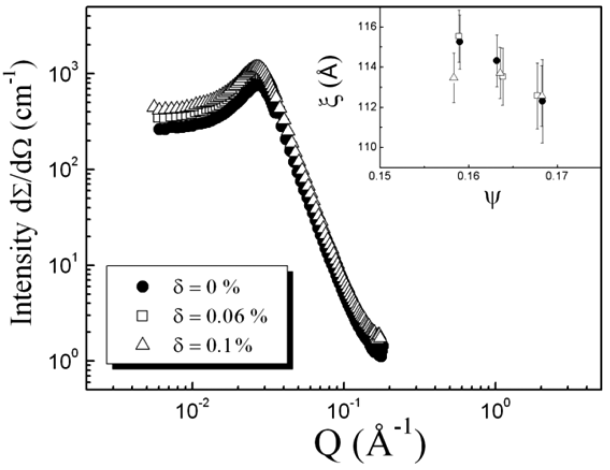

Figure 10. SANS spectra for C12−D_2O−$C_{10}E_4$−$PEP_{22}PEO_{22}$ systems with different polymer contents and $\gamma = 0.175$. No variation of the peak width as we add polymer is visible. This means no variation of the correlation length as shown in the inset.

On the basis of these measurements, we can classify our systems in two main classes. The first one comprises the shorter chain oils. There the polymer finds a favorable environment and acts as "booster", increasing the stiffness of the membrane and rendering it flatter (long correlation lengths), while for the second class, comprising the longer chain oils, the polymer acts like "anti-booster". It cannot prevent the softening of the membrane due to the thermal fluctuations and the correlation lengths will be shorter (for flabby interfaces correlated points lie closer to each other).

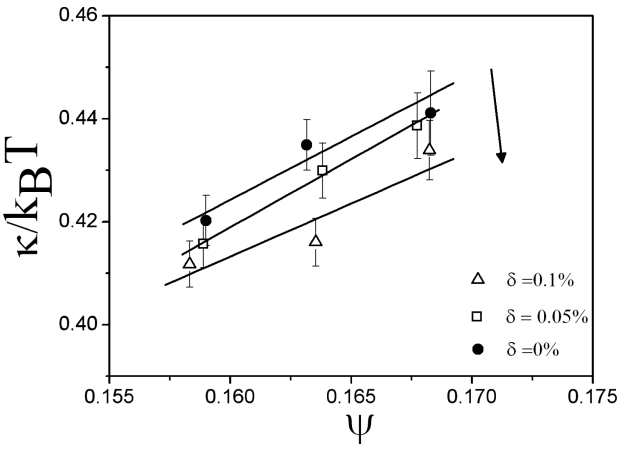

Figure 11. Renormalized bending rigidity obtained by SANS measurements for C12−D_2O−$C_{10}E_4$−$PEP_{22}PEO_{22}$ systems at different polymer contents as a function of the membrane volume fraction.

DISCUSSION

In this section we discuss the effect of diblock copolymers on the bending rigidity κ and the saddle-splay modulus $\bar{\kappa}$; i.e., we will comment on the sensitivities Ξ, $\bar{\Xi}$ of κ and $\bar{\kappa}$ respectively, obtained by SANS and phase diagram measurements, in terms of the inverse of confinement d/R_{ee}. As already mentioned in the Introduction, we qualitatively expect three well-defined regimes: a low-confinement regime where the length of the polymer is smaller than domain size characterized by an increase by the anchored diblock copolymer, a medium-confinement regime where the polymer size is comparable to the microemulsion structure size and where the boosting effect is enhanced, and high-confinement regime where the polymer larger than the oil/water domains for that a decrease of the effective membrane bending rigidity is found.

We considered for our calculations the average R_{ee} as the confinement in one domain involves only one block and d specifies the domain size of a *single* domain contrary to the Teubner−Strey formula domain size d_{TS}, which measures the domain spacing of consecutive identical domains, and thus $d = (1/2)d_{TS}$. Through the Gaussian random field theory we calculate the bending rigidity from the domain size d and the correlation length ξ obtained by fitting the SANS spectra. We measured many microemulsions: for every value of confinement we established three different polymer contents (among these even the value zero corresponding to the pure system). For every polymer content we prepared three samples with different membrane content. The bending rigidity, interpolated at constant Ψ, as a function of the polymer content follows a linear behavior. The slope obtained from the fit is proportional to the sensitivity coefficient Ξ:

$$\frac{\Delta\kappa_R}{k_B T} = \Xi\sigma(R_O + R_W)^2$$

In Figure 12 the experimental and simulated Ξ are shown as function of the inverse of confinement in the case of the diblock copolymers. In the interval $1 < d/R_{ee} < 2.5$, a constant Ξ about 2 times the analytical value is obtained that agrees with the value 0.334 found in the literature[3,30] for $d/R_{ee} \sim 3$. But when the domain size is comparable to the end-to-end distance of the polymer, the sensitivity starts to diminish, going down to negative values until it diverges for high confinement ($d/R_{ee} < 1$).

dx.doi.org/10.1021/jp402825d | J. Phys. Chem. B XXXX, XXX, XXX−XXX

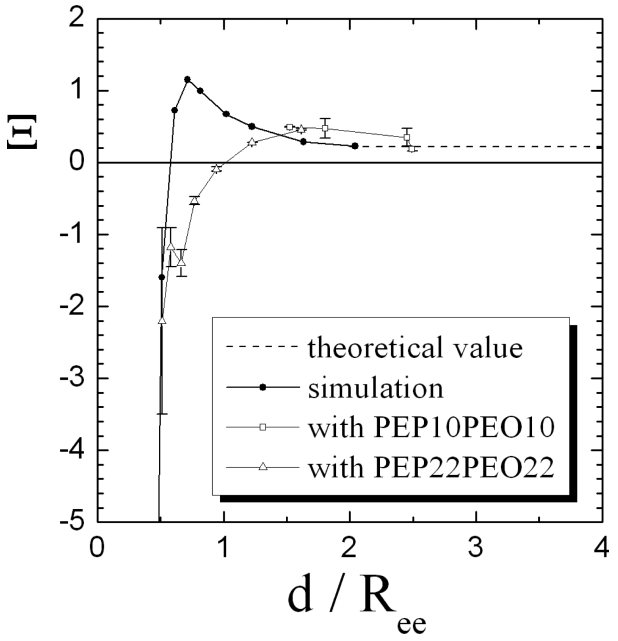

Figure 12. Sensitivity coefficient of the bending rigidity for the diblock copolymers derived from SANS measurements as function of the inverse of confinement.

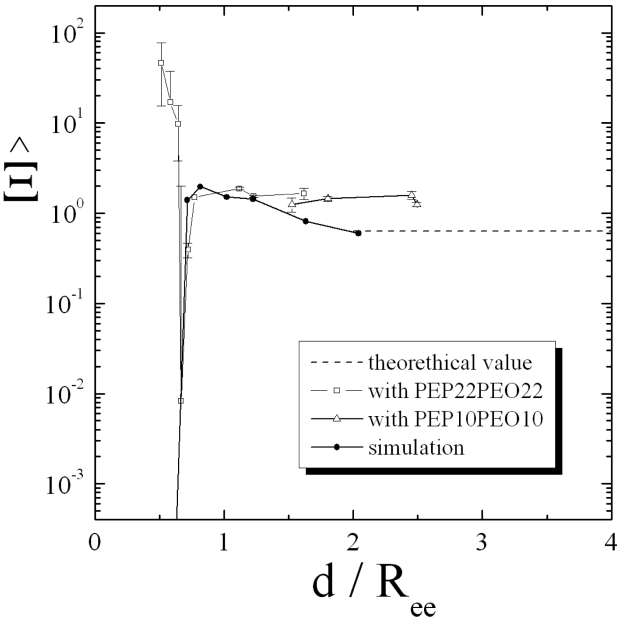

Figure 13. Sensitivity coefficient of the saddle-splay modulus for the diblock copolymers calculated from the phase diagram measurements as function of the inverse of confinement.

The simulation predicts a different behavior in the region of medium confinement. There a grow starts at $d/R_{ee} = 2$ and reaches a strong peak placed at 0.7. The reversed behavior at high confinement is confirmed by our measurements.

It was introduced by eq 4 how the saddle-splay modulus is related to the membrane volume fraction at the FTP, and in eq 7 we saw how to relate the membrane volume fraction with the polymer grafting density:

$$\ln\left(\frac{\tilde{\Psi}}{\tilde{\Psi}^0}\right) = -\hat{\Xi}\sigma(R_W^2 + R_O^2)$$

with $\tilde{\Psi}^0 = \exp(6\pi\bar{\kappa}_0/5k_BT)$ being the intrinsic membrane concentration of the pure system. $\tilde{\Psi}$ was obtained from the phase diagram measurements and plotted logarithmically as a function of the product $\sigma(R_W^2 + R_O^2)$. The resulting linear dependence can be easily fitted giving us a slope corresponding to the sensitivity coefficient $\hat{\Xi}$.

In Figure 13 the $\hat{\Xi}$ values are plotted versus the inverse of confinement. The open symbols represent the experimental points in comparison with the simulation (full symbol).

We found a positive constant value around $\hat{\Xi} = 1.51$ in perfect agreement with previous work,[3] for a wide range of d/R_{ee} between 2.5 and 0.7. The positive value of the sensitivity indicates an increase of the absolute value of $\bar{\kappa}$ with the addition of polymer. Energetically speaking, it is less expensive to create a saddle-type deformation of the membrane. The one-phase region is more stable and requires less surfactant (decreasing ln Ψ). Like it happened with κ, the amplitude of the diblock copolymers influence on $\bar{\kappa}$ is found to be about double of the analytical value but it stays constant between low and medium confinement. Then, when the polymer size becomes larger than the domain size ($d/R_{ee} = 0.7$), we enter the high confinement, observing a steep drop down to small values again in good agreement with the simulation. Nevertheless, the last points at very high confinement experience a huge positive value that may be explained as due to the osmotic pressure of the polymer on the membrane.[31] In the whole interpretation of the data, this pressure was neglected.

For both the coefficients Ξ and $\hat{\Xi}$, we observed the same qualitative behavior: a constant positive value that, at a certain degree of confinement defining the boundary between the high and medium regime, tends to fall toward negative values. The decrease of Ξ happens in a more soft way than for $\hat{\Xi}$ which has a real sudden drop down and it starts earlier at a higher value of d/R_{ee}.

Diblock copolymers are flexible *macro*surfactant molecules with a non-negligible volume. So when the domain size starts to be comparable with the end-to-end distance it might be necessary to take into account a *depletion* of the polymer chain involving the anchoring and surrounding membranes. The consequence is that the polymer would be not so present on the surface as predicted by the simulation and it could justify why the polymer boosting effect, i.e., the positive values of Ξ and $\hat{\Xi}$, are not growing but stay constant. This hypothesis is supported by previous SANS experiments[32] performed on oil-in-water droplet microemulsions decorated by diblock copolymers. The analysis of the partial scattering functions, obtained by the use of different contrasts, revealed a sphere−shell−shell structure of the droplets: the inner core consists of oil surrounded by a shell of surfactant. Then a second shell surrounds the whole droplet where the polymer density is lower than beyond this shell. The size of this second shell, interpreted like a depletion zone, was found to be comparable with the droplet radius. While the experiments found a rather large depletion zone for little confinement, a qualitatively similar picture was found by Laradji[33] for anchored polymers in the brush regime. The brushlike confinement of the polymers induces the polymer to be more stretched in the vicinity of the membrane than what would be expected in the presence of the solvent. Laradji says that the polymer has a more blendlike character. This finding is supported by a theory of Gompper[34] where the polymer blends are described. The resulting sensitivities Ξ and $\hat{\Xi}$ are more likely reduced than increased.

dx.doi.org/10.1021/jp402825d | J. Phys. Chem. B XXXX, XXX, XXX−XXX

Furthermore, the spectra of decorated droplets in shell contrast show evidence of a repulsive interaction between the droplets induced by the corona of PEO.[35] Therefore, it seems plausible to consider around the polymer chains a depletion shell that avoid a more and more enhanced boosting effect on the membrane. However, it is important to note that we do not consider the polymer like a hard-sphere colloid because if it was so, we would have observed a variation of the domain size with the polymer concentration for the formation of bulges.

As another point, we tried to explain why Ξ decays earlier than $\hat{\Xi}$. This may be explained considering the structure of the bicontinuous phase as a network of oil and water cylindrical channels with a certain mean curvature H and Gaussian curvature $K = 0$. Moreover, oil or water channels are connected to each other by junctions where the presence of saddle-splay deformations on the membrane implies $K \neq 0$. The polymers in the channels will contribute to κ and those located in the junctions will contribute to $\bar{\kappa}$. For the same value of confinement, the cylinder parts of the domains have less space available for the polymer than in the junctions. So the antiboosting effect will appear earlier in κ than in $\bar{\kappa}$.

At this point we would like to compare the confinement measurements of diblock copolymers with homopolymers. The bare sensitivity coefficient β of homopolymer additive is shown in Figure 14. Similarly to diblock copolymers, it is defined by

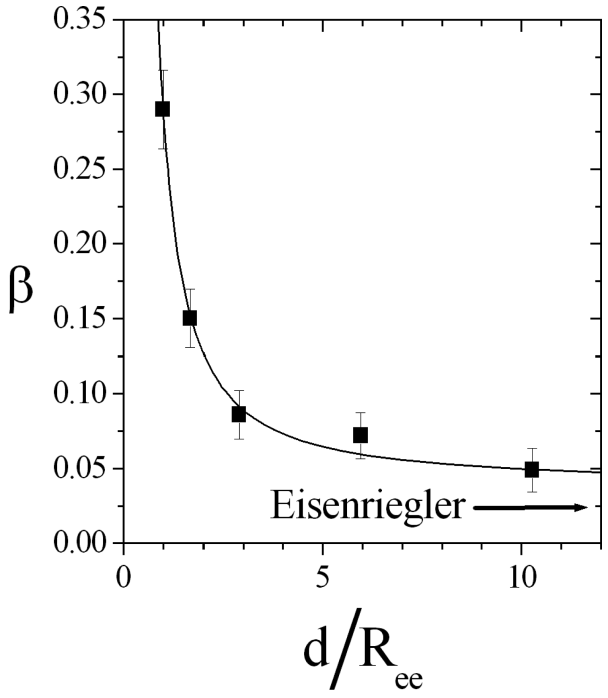

Figure 14. Sensitivity coefficient of the bending rigidity for homopolymers derived from SANS measurements as function of the inverse of confinement.

the change of the bending rigidity $\Delta\kappa = -\beta(\phi_H/V_H)(R_{HW}^3 + R_{OH}^3)$ with the theoretical coefficient $\beta = 0.0238$ from the theory of Eisenriegler[36] (with the polymer concentration ϕ_H, the polymer molecular volume V_H, and the end-to-end distances of the water and oil soluble homopolymers R_{HW} and R_{HO}). Experimentally, the coefficient takes double the value at low confinement (large $d/R_{ee} \sim 10$). The confinement effect results in a clear elevation of the β-parameter by amplifications of up to 6 times. There is no change in sign as for the diblock copolymers, so the confinement effect of homopolymers has a less complicated effect as diblock copolymers with only two regions of low confinement and strong confinement. The confinement of homopolymers results in a stronger antiboosting, similar to the diblock copolymers and no change in sign is needed. The description of strong confinement for any kind of polymers[37] finally finds that the multiple reflections of the polymer by the membrane do not depend on the single anchoring of polymer anymore. The original β-parameter is therefore scaled to units of the Ξ-parameter in Figure 15

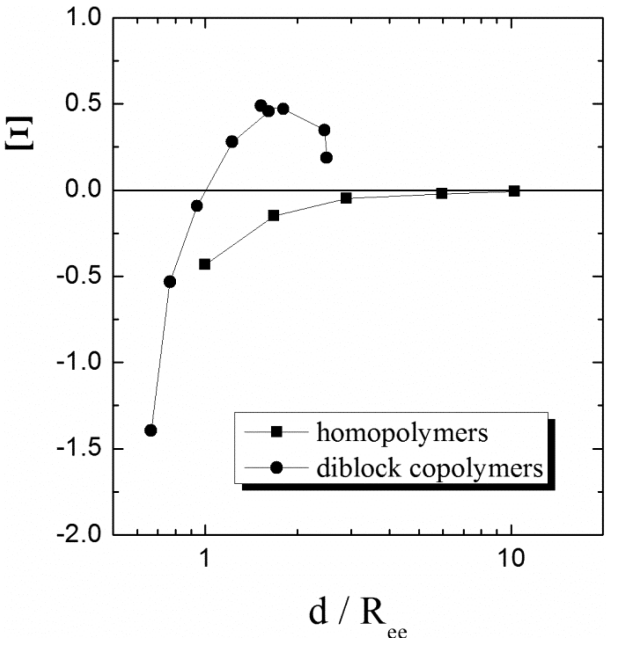

Figure 15. Comparison of sensitivity coefficient of the bending rigidity for the diblock copolymers for homopolymers as function of the inverse of confinement.

according to $\Xi_{eff} = -\beta\Psi R_{ee}/a$ (with the surfactant concentration Ψ, the average end-to-end distance R_{ee}, and the surfactant film thickness a). The same orders of magnitude are reached at confinement values of $d/R_{ee} \approx 1$. To some extent, we can claim that the high-confinement region would be identical for homopolymers and diblock copolymers.

CONCLUSIONS

Bicontinuous microemulsions consisting of water, oil, nonionic surfactant, and polymer were the subject of our work. In particular, our purpose was to explain how the polymer, confined between the surfactant interfaces, can influence the structure and phase behavior.

The combination of studies of the macroscopic phase behavior on one side and the microscopic structure by SANS experiments on the other side permitted us to have access to the knowledge of several quantities connected to the Helfrich model. The sensitivities of fundamental parameters like the bending rigidity and the saddle-splay modulus to polymer addition were investigated. The importance to understand their behavior relies on the large variety of applications that these systems have in everyday life.

The influence due to addition of diblock copolymer additives on the properties of the microemulsion depends on the geometry of the microemulsion itself. The confinement can

dx.doi.org/10.1021/jp402825d | J. Phys. Chem. B XXXX, XXX, XXX−XXX

modify the *pure* polymer effect. If the ratio between the two dimensions of the polymer and of the microemulsion is maintained greater than 1, we observed the predominant boosting effect until the confinement increases when we pass from low to medium regime. Here we argue that some depletion effects become important and limit the action of the polymer avoiding the strong peak found in the simulation. Finally, when d and R_{ee} are comparable (high confinement), the sensitivities of the bending rigidity and saddle-splay modulus diverge.

■ ASSOCIATED CONTENT

Supporting Information

Evaluation of the SANS bending rigidity κ_{SANS} in terms of κ and $\bar{\kappa}$, and corrected coefficient Ξ as function of confinement. This material is available free of charge via the Internet at http://pubs.acs.org.

■ AUTHOR INFORMATION

Corresponding Author

*Tel.: +49-89-289-13805. Fax: +49-89-289-10799. E-mail: s.maccarrone@fz-juelich.de.

Notes

The authors declare no competing financial interest.

■ REFERENCES

(1) Safran, S. A. *Statistical thermodynamics of surfaces, interfaces, and membranes*; Addison-Wesley: Reading, MA, 1994.
(2) Jakobs, B.; Sottmann, T.; Strey, R.; Allgaier, J.; Willner, L.; Richter, D. *Langmuir* **1999**, *15*, 6707−6711.
(3) Endo, H.; Allgaier, J.; Gompper, G.; Jakobs, B.; Monkenbusch, M.; Richter, D.; Sottmann, T.; Strey, R. *Phys. Rev. Lett.* **2000**, *85*, 102−105.
(4) Endo, H.; Mihailescu, M.; Monkenbusch, M.; Allgaier, J.; Gompper, G.; Richter, D.; Jakobs, B.; Sottmann, T.; Strey, R.; Grillo, I. *J. Chem. Phys.* **2001**, *115*, 580−600.
(5) Byelov, D.; Frielinghaus, H.; Holderer, O.; Allgaier, J.; Richter, D. *Langmuir* **2004**, *20*, 10433−10443.
(6) Auth, T.; Gompper, G. *Phys. Rev. E* **2003**, *68*, 051801.
(7) Auth, T.; Gompper, G. *Phys. Rev. E* **2005**, *72*, 031904.
(8) Helfrich, W. *Z. Naturforsch.* **1973**, *28c*, 693−703.
(9) Peliti, L.; Leibler, S. *Phys. Rev. Lett.* **1985**, *54*, 1690−1693.
(10) Hiergeist, C.; Lipowsky, R. *J. Phys. II Fr.* **1996**, *6*, 1465−1481.
(11) Eisenriegler, E.; Hanke, A.; Dietrich, S. *Phys. Rev. E* **1996**, *54*, 1134−1152.
(12) Breidenich, M.; Netz, R. R.; Lipowsky, R. *Mol. Phys.* **2005**, *103*, 3169−3183.
(13) Bickel, T.; Marques, C. M. *Eur. Phys. J., E* **2002**, *9*, 349−352.
(14) Leibler, S. *J. Phys. (Paris)* **1986**, *47*, 507−516.
(15) Sottmann, T. Ph.D. Dissertation; Georg-August Universität zu Göttingen: Göttingen, Germany, 1997.
(16) Allgaier, J.; Poppe, A.; Willner, L.; Richter, D. *Macromolecules* **1997**, *30*, 1582−1586.
(17) PEP in cyclohexane: Mays, J. W.; Fetters, L. J. *Macromolecules* **1989**, *22*, 921−926. PEO in water: Kawaguchi, S.; Imai, G.; Suzuki, J.; Miyahara, A.; Kitano, T.; Ito, K. *Polymer* **1997**, *38*, 2885−2891.
(18) Morse, C. *Phys. Rev. E* **1994**, *50*, R2423−R2426.
(19) Gompper, G.; Kroll, D. M. *Phys. Rev. Lett.* **1998**, *81*, 2284−2287.
(20) Kahlweit, M.; Strey, R.; Haase, D.; Kunieda, H.; Schmeling, T.; Faulhaber, B.; Borkovec, M.; Eicke, H.-F.; Busse, G.; Eggers, F.; Funk, Th.; Richmann, H.; Magid, L.; Sönderman, O.; Stilbs, P.; Winkler, J.; Dittrich, A.; Jahn, W. *J. Colloid Interface Sci.* **1987**, *118*, 436−453.
(21) Teubner, M.; Strey, R. *J. Chem. Phys.* **1987**, *87*, 3195−3200.
(22) Pieruschka, P.; Safran, S. A. *Europhys. Lett.* **1993**, *22*, 625−630.
(23) Pieruschka, P.; Safran, S. A. *Europhys. Lett.* **1995**, *31*, 207−212.
(24) Peltomäki, M.; Gompper, G.; Kroll, D. *J. Chem. Phys.* **2012**, *136*, 134708.
(25) Holderer, O.; Frielinghaus, H.; Monkenbusch, M.; Klostermann, M.; Sottmann, T.; Richter, D. *Soft Matter* **2012**, *9*, 2308−2313.
(26) Pedersen, J. S.; Posselt, D.; Mortensen, K. *J. Appl. Crystallogr.* **1990**, *23*, 321−333.
(27) Sottmann, T.; Strey, R. *J. Chem. Phys.* **1997**, *106*, 8606−8615.
(28) Sottmann, T.; Strey, R. *J. Chem. Phys.* **1997**, *106*, 6483−6491.
(29) Frank, C. Ph.D. Dissertation; Universität zu Köln: Köln, Germany, 2004.
(30) Gompper, G.; Endo, H.; Mihailescu, M.; Allgaier, J.; Monkenbusch, M.; Richter, D.; Jakobs, B.; Sottmann, T.; Strey, R. *Europhys. Lett.* **2001**, *56*, 683−689.
(31) Bouglet, G.; Ligoure, C. *Eur. Phys. J. B* **1999**, *9*, 137−147.
(32) Frielinghaus, H.; Byelov, D.; Allgaier, J.; Monkenbusch, M.; Richter, D.; Jakobs, B.; Sottmann, T.; Strey, R. *Appl. Phys. A: Mater. Sci. Process.* **2002**, *74*, S408−S410.
(33) Laradji, M. *Europhys. Lett.* **2002**, *60*, 594−600.
(34) Müller, M.; Gompper, G. *Phys. Rev. E* **2002**, *66*, 041805(1)−041805(13).
(35) Appell, J.; Ligoure, C.; Porte, G. *J. Stat. Mech.: Theor. Exp.* **2004**, P08002(1)−P08002(14).
(36) Hanke, A.; Eisenriegler, E.; Dietrich, S. *Phys. Rev. E* **1999**, *59*, 6853−6878.
(37) Dotera, T.; Suzuki, Y. *Phys. Rev. E* **2000**, *62*, 5318−5323.